

# Riemann zeros and periodic orbit quantization by harmonic inversion

Jörg Main <sup>†</sup>, Vladimir A. Mandelshtam <sup>‡</sup>, Günter Wunner <sup>†</sup>, and  
Howard S. Taylor <sup>‡</sup>

<sup>†</sup> Theoretische Physik I, Ruhr-Universität Bochum, D-44780 Bochum, Germany

<sup>‡</sup> University of Southern California, Department of Chemistry, Los Angeles, CA 90089

**Abstract.** In formal analogy with Gutzwiller's semiclassical trace formula, the density of zeros of the Riemann zeta function  $\zeta(z = \frac{1}{2} - iw)$  can be written as a non-convergent series  $\varrho(w) = -\pi^{-1} \sum_p \sum_{m=1}^{\infty} \ln(p) p^{-m/2} \cos(wm \ln(p))$  with  $p$  running over the prime numbers. We obtain zeros and poles of the zeta function by harmonic inversion of the "time" signal which is a Fourier transform of  $\varrho(w)$ . More than 2500 zeros have been calculated to about 12 digit precision as eigenvalues of small matrices using the method of filter-diagonalization. Due to formal analogy of the zeta function with Gutzwiller's periodic orbit trace formula, the method can be applied to the latter to accurately calculate individual semiclassical eigenenergies and resonance poles for classically chaotic systems. The periodic orbit quantization is demonstrated on the three disk scattering system as a physical example.

PACS numbers: 03.65.Sq, 05.45.+b, 02.30.Px

Short title: Riemann zeros and periodic orbit quantization by harmonic inversion

June 4, 1997

## 1. Introduction

Since the development of *periodic orbit theory* by Gutzwiller [1, 2] it has become a fundamental question as to how individual semiclassical eigenenergies and resonances can be obtained from periodic orbit quantization for classically chaotic systems. A major problem is the exponential proliferation of the number of periodic orbits with increasing period, resulting in a divergence of Gutzwiller's trace formula at real energies and below the real axis, where the poles of the Green's function are located. To extract individual eigenstates the semiclassical trace formula has to be analytically continued to the region of the quantum poles, which can be achieved for some systems, e.g., by cycle expansion techniques [3].

Analytic continuation is also a well known problem for certain representations of the famous Riemann zeta function [4]. As pointed out by Berry [5] the density of zeros of Riemann's zeta function can be written, in formal analogy with Gutzwiller's semiclassical trace formula, as a non-convergent series, where the "periodic orbits" are the prime numbers. Therefore the Riemann zeta function has served as a mathematical model for quantum systems with an underlying chaotic classical dynamics for both the development of semiclassical techniques [5, 6, 7] and the study of statistical properties of level distributions [8, 9, 10].

In this paper we present a new technique for the calculation of Riemann zeros based on *harmonic inversion*. The advantage of the method is that it does not depend on special properties of the zeta function, such as the functional equation [4], and therefore can be generalized in a natural way to overcome the convergence problem of Gutzwiller's periodic orbit sum, and thus to calculate semiclassical eigenenergies and resonance poles of classically chaotic systems by harmonic inversion of the periodic orbit recurrence function.

The paper is organized as follows. In Section 2 we explain the general idea of the method by way of example of the Riemann zeros. It is followed by the derivation of our harmonic inversion method in Section 3 and the presentation of numerical results for the Riemann zeros in Section 4. The method is extended to the general case of periodic orbit quantization in Section 5 and its usefulness demonstrated for the three disk scattering system, as a physical example, in Section 6.

## 2. The Riemann zeta function

Our goal is to introduce our method for periodic orbit quantization using, as an example, the well defined problem of calculating zeros of the Riemann zeta function. There are essentially two advantages of studying the zeta function. First, the Riemann analogue of Gutzwiller's trace formula is exact, whereas in periodic orbit theory the semiclassical

trace formula is correct only to first order in  $\hbar$ . This allows a direct check on the precision of the method. Second, no extensive periodic orbit search is necessary for the calculation of Riemann zeros, as the only input data are just prime numbers. Before discussing our method we start with recapitulating a few brief remarks on Riemann's zeta function necessary for our purposes.

### 2.1. General remarks

The hypothesis of Riemann is that all the non-trivial zeros of the analytic continuation of the function

$$\zeta(z) = \sum_{n=1}^{\infty} n^{-z} = \prod_p (1 - p^{-z})^{-1}, \quad (\text{Re } z > 1, p : \text{primes}) \quad (1)$$

have real part  $\frac{1}{2}$ , so that the values  $w = w_k$ , defined by

$$\zeta\left(\frac{1}{2} - iw_k\right) = 0, \quad (2)$$

are all real or purely imaginary [4]. The Riemann staircase function for the zeros along the line  $z = \frac{1}{2} - iw$ , defined as

$$N(w) = \sum_{k=1}^{\infty} \Theta(w - w_k), \quad (3)$$

i.e. the number  $N(w)$  of zeros with  $w_k < w$ , can be split [4, 5] into a smooth part,

$$\overline{N}(w) = \frac{w}{2\pi} \left( \ln \left\{ \frac{w}{2\pi} \right\} - 1 \right) + \frac{7}{8}, \quad (4)$$

and a fluctuating part,

$$N_{\text{osc}}(w) = -\frac{1}{\pi} \lim_{\eta \rightarrow 0} \text{Im} \ln \zeta \left( \frac{1}{2} - i(w + i\eta) \right). \quad (5)$$

Substituting the product formula (1) (assuming that it can be used when  $\text{Re } z = \frac{1}{2}$ ) into (5) and expanding the logarithms gives

$$N_{\text{osc}}(w) = -\frac{1}{\pi} \text{Im} \sum_p \sum_{m=1}^{\infty} \frac{1}{mp^{m/2}} e^{iwm \ln(p)}. \quad (6)$$

Therefore the density of zeros along the line  $z = \frac{1}{2} - iw$  can formally be written as

$$\varrho_{\text{osc}}(w) = \frac{dN_{\text{osc}}}{dw} = -\frac{1}{\pi} \text{Im } g(w) \quad (7)$$

with the response function  $g(w)$  given by the series

$$g(w) = i \sum_p \sum_{m=1}^{\infty} \frac{\ln(p)}{p^{m/2}} e^{iwm \ln(p)}, \quad (8)$$

which converges only for  $\text{Im } w > \frac{1}{2}$ .

As has been pointed out by Berry [5, 6] the above equation has the same mathematical form as Gutzwiller's semiclassical trace formula, where the fluctuating part of the density of states  $\varrho_{\text{osc}}(E)$  of a quantum system is expressed as the periodic orbit sum

$$\varrho_{\text{osc}}(E) \approx -\frac{1}{\pi} \text{Im} \sum_{\text{po}} A_{\text{po}} e^{iS_{\text{po}}}, \quad (9)$$

where  $A_{\text{po}}$  are the amplitudes and  $S_{\text{po}}$  the classical actions (including phase information) of the periodic orbit contributions. For the Riemann zeta function the primitive periodic orbits have to be identified with the primes  $p$ . The amplitudes and actions are then given by

$$A_{pm} = i \frac{\ln(p)}{p^{m/2}}, \quad (10)$$

$$S_{pm} = mw \ln(p). \quad (11)$$

Both equations (7) for the Riemann zeros and – for most classically chaotic physical systems – the periodic orbit sum (9) do not converge. In particular, zeros of the zeta function, or semiclassical eigenstates, cannot be obtained directly using these expressions. The problem is to find the analytic continuation of these equations to the region where the Riemann zeros or, for physical systems, the eigenenergies and resonances are located.

For the Riemann zeta function it follows from the functional equation [4] that the function

$$Z(w) = \exp \left\{ -i \left[ \arg \Gamma \left( \frac{1}{4} + \frac{1}{2} iw \right) - \frac{1}{2} w \ln \pi \right] \right\} \zeta \left( \frac{1}{2} - iw \right) \quad (12)$$

is real and even for real  $w$ . The asymptotic representation of  $Z(w)$  for large  $w$ ,

$$Z(w) \approx -2 \sum_{n=1}^{\text{Int}[\sqrt{w/2\pi}]} \frac{\cos\{\pi \bar{N}(w) - w \ln n\}}{n^{1/2}}, \quad (13)$$

is known as the Riemann-Siegel formula and has been employed (with several correction terms) in effective methods for computing Riemann zeros [9].

The Riemann-Siegel formula (13) has been used as the starting point to develop a “rule for quantizing chaos” and to derive an approximate “semiclassical functional equation” [6, 7]. However, the semiclassical functional equation can only be applied to bound systems with real eigenvalues, and the concept requires the introduction of *pseudo-orbits*.

The main goal of this paper is to demonstrate that Riemann zeros can be obtained directly from the “ingredients” of the non-convergent response function (8), i.e., the set of values  $A_{pm}$  and  $S_{pm}$ , thus avoiding the use of the functional equation, the Riemann-Siegel formula, or any other special property of the zeta function. Because of the formal

equivalence between Eqs. (7) and (9) our method can then be applied for periodic orbit quantization of classically chaotic systems [11] without any modification.

## 2.2. The ansatz for the Riemann zeros

To find the analytic continuation of Eq. (8) in the region  $\text{Im } w < \frac{1}{2}$  we essentially want to fit  $g(w)$  to its exact functional form,

$$g_{\text{ex}}(w) = \sum_k \frac{d_k}{w - w_k + i\epsilon}, \quad (14)$$

arising from the definition of the Riemann staircase (3). The “multiplicities”  $d_k$  in Eq. 14 are formally the fitting parameters, although here they should be all equal to 1.

It is hard to directly fit the non-convergent (on the real axis) series  $g(w)$  to the form of  $g_{\text{ex}}(w)$ . The first step towards the solution of the problem is to carry out the above fitting problem for the Fourier components of the response function,

$$C(s) = \frac{1}{2\pi} \int_{-\infty}^{+\infty} g(w) e^{-isw} dw = i \sum_p \sum_{m=1}^{\infty} \frac{\ln(p)}{p^{m/2}} \delta(s - m \ln(p)), \quad (15)$$

which after certain regularization (see below) is a well behaved function of  $s$ . Due to the formal analogy with periodic orbit theory (see Eqs. 10 and 11),  $C(s)$  can be interpreted as the recurrence function for the Riemann zeta function with the recurrence positions  $S_{pm} = m \ln(p)$  and recurrence strengths of periodic orbit recurrences  $A_{pm} = i \ln(p) p^{-m/2}$ . The exact functional form which now should be used to fit the  $C(s)$  is given by

$$C_{\text{ex}}(s) = \frac{1}{2\pi} \int_{-\infty}^{+\infty} g_{\text{ex}}(w) e^{-isw} dw = -i \sum_{k=1}^{\infty} d_k e^{-iw_k s}. \quad (16)$$

$C_{\text{ex}}(s)$  is a superposition of sinusoidal functions with frequencies  $\dagger w_k$  given by the Riemann zeros and amplitudes  $d_k = 1$ .

Fitting a signal  $C(s)$  to the functional form of Eq. (16) with, in general, both complex frequencies  $w_k$  and amplitudes  $d_k$  is known as *harmonic inversion*, with a large variety of applications in various fields [12, 13, 14, 15, 16]. The harmonic inversion analysis is especially non-trivial if the number of frequencies in the signal  $C(s)$  is large, e.g., more than a thousand. It is additionally complicated by the fact that the conventional way to perform the spectral analysis by studying the Fourier spectrum of  $C(s)$  will bring us back to analyzing the non-convergent response function  $g(w)$  defined in Eq. 8. As such until recently the known techniques of spectral analysis would not be applicable in the present case. It is the filter-diagonalization method [13, 14] which made the harmonic inversion concept a general and powerful computational tool.

$\dagger$  It is convenient to use the word “frequencies” for  $w_k$  referring to the sinusoidal form of  $C(s)$ . We will also use the word “poles” in the context of the response function  $g(w)$ .

The signal  $C(s)$  as defined by Eq. 15 is not yet suitable for the spectral analysis. The next step is to regularize  $C(s)$  by convoluting it with a Gaussian to obtain the smoothed signal,

$$\begin{aligned} C_\sigma(s) &= \frac{1}{\sqrt{2\pi}\sigma} \int_{-\infty}^{+\infty} C(s') e^{-(s-s')^2/2\sigma^2} ds' \\ &= \frac{i}{\sqrt{2\pi}\sigma} \sum_p \sum_{m=1}^{\infty} \frac{\ln(p)}{p^{m/2}} e^{-(s-m\ln(p))^2/2\sigma^2}, \end{aligned} \quad (17)$$

that has to be fit to the corresponding convolution of  $C_{\text{ex}}(s)$ . The latter is readily obtained by substituting  $d_k$  in Eq. 16 by the damped amplitudes,

$$d_k \rightarrow d_k^{(\sigma)} = d_k e^{-w_k^2 \sigma^2 / 2}. \quad (18)$$

As such the regularization can also be interpreted as a cut of an infinite number of high frequencies in the signal which is of fundamental importance for a numerically stable harmonic inversion.

Before proceeding further we note that even though the derivation of Eq. 17 assumed that the zeros  $w_k$  are on the real axis, the analytic properties of  $C_\sigma(s)$  imply that its representation by Eq. 17 includes not only the non-trivial real zeros, but also all the trivial ones,  $w_k = -i(2k + \frac{1}{2})$ ,  $k = 1, 2, \dots$ , which are purely imaginary. The general harmonic inversion procedure described below does not require the frequencies to be real. As such both the real and imaginary zeros  $w_k$  will be obtained as the eigenvalues of a non-Hermitian generalized eigenvalue problem.

### 3. Filter-diagonalization method for harmonic inversion

The harmonic inversion problem can be formulated as a non-linear fit (see, e.g., Ref. [12]) of the signal  $C(s)$  defined on an equidistant grid,

$$c_n \equiv C(n\tau) = \sum_k d_k e^{-in\tau w_k}, \quad n = 0, 1, 2, \dots, N, \quad (19)$$

with the set of generally complex variational parameters  $\{w_k, d_k\}$ . (In this context the Discrete Fourier Transform scheme would correspond to a linear fit with  $N$  amplitudes  $d_k$  and fixed real frequencies  $w_k = 2\pi k/N\tau$ ,  $k = 1, 2, \dots, N$ . The latter implies the so called “uncertainty principle”, i.e., the resolution, defined by the Fourier grid spacing,  $\Delta w$ , is inversely proportional to the length,  $s_{\text{max}} = N\tau$ , of the signal  $C(s)$ .) The “high resolution” property associated with Eq. 19 is due to the fact that there is no restriction for the closeness of the frequencies  $w_k$  as they are variational parameters. In Ref. [13] it was shown how this non-linear fit problem can be recasted as a linear algebraic one using the filter-diagonalization procedure. The essential idea was to associate the signal  $c_n$  with an autocorrelation function of a suitable dynamical system,

$$c_n = \left( \Phi_0, \hat{U}^n \Phi_0 \right), \quad (20)$$

where  $(\cdot, \cdot)$  defines a complex symmetric inner product (i.e., no complex conjugation). The evolution operator can be defined implicitly by

$$\hat{U} \equiv e^{-i\hat{\Omega}} = \sum_{k=1}^K e^{-i\omega_k} |\Upsilon_k\rangle\langle\Upsilon_k|, \quad (21)$$

where the set of eigenvectors  $\{\Upsilon_k\}$  is associated with an arbitrary orthonormal basis set and the eigenvalues of  $\hat{U}$  are  $u_k \equiv e^{-i\omega_k}$  (or equivalently the eigenvalues of  $\hat{\Omega}$  are  $\omega_k$ ). Inserting Eq. 21 into Eq. 20 we obtain Eq. 19 with

$$d_k = (\Upsilon_k, \Phi_0)^2, \quad (22)$$

which also implicitly defines the “initial state”  $\Phi_0$ .

This construction establishes an equivalence between the problem of extracting spectral information from the signal with the one of diagonalizing the evolution operator  $\hat{U} = e^{-i\tau\hat{\Omega}}$  (or the Hamiltonian  $\hat{\Omega}$ ) of the fictitious underlying dynamical system. The filter-diagonalization method is then used for extracting the eigenvalues of the Hamiltonian  $\hat{\Omega}$  in any chosen small energy window. Operationally this is done by solving a small generalized eigenvalue problem whose eigenvalues yield the frequencies in a chosen window. The knowledge of the operator  $\hat{\Omega}$  itself is not required, as for a properly chosen basis the matrix elements of  $\hat{\Omega}$  can be expressed only in terms of  $c_n$ . The advantage of the filter-diagonalization procedure is its numerical stability with respect to both the length and complexity (the number and density of the contributing frequencies) of the signal. Here we apply the method of Ref. [14] which is an improvement of the filter-diagonalization method of Ref. [13] in that it allows to significantly reduce the required length of the signal by implementing a different Fourier-type basis with an efficient rectangular filter. Such a basis is defined by choosing a small set of values  $\varphi_j$  in the frequency interval of interest,  $\tau\omega_{min} < \varphi_j < \tau\omega_{max}$ ,  $j = 1, 2, \dots, J$ , and the maximum order,  $M$ , of the Krylov vectors,  $\Phi_n = e^{-in\tau\hat{\Omega}}\Phi_0$ , used in the Fourier series,

$$\Psi_j \equiv \Psi(\varphi_j) = \sum_{n=0}^M e^{in\varphi_j} \Phi_n \equiv \sum_{n=0}^M e^{in(\varphi_j - \tau\hat{\Omega})} \Phi_0. \quad (23)$$

It is convenient to introduce the notations,

$$U_{jj'}^{(p)} \equiv U^{(p)}(\varphi_j, \varphi_{j'}) = \left( \Psi(\varphi_j), e^{-ip\tau\hat{\Omega}} \Psi(\varphi_{j'}) \right), \quad (24)$$

for the matrix elements of the operator  $e^{-ip\tau\hat{\Omega}}$ , and  $\mathbf{U}^{(p)}$ , for the corresponding small  $J \times J$  complex symmetric matrix. As such  $\mathbf{U}^{(1)}$  denotes the matrix representation of the operator  $\hat{U}$  itself and  $\mathbf{U}^{(0)}$ , the overlap matrix with elements  $(\Psi(\varphi_j), \Psi(\varphi_{j'}))$ , which is required as the vectors  $\Psi(\varphi_j)$  are not generally orthonormal. Now using these definitions we can set up a generalized eigenvalue problem,

$$\mathbf{U}^{(p)} \mathbf{B}_k = e^{-ip\tau\omega_k} \mathbf{U}^{(0)} \mathbf{B}_k, \quad (25)$$

for the eigenvalues  $e^{-ip\omega_k}$  of the operator  $e^{-ip\tau\hat{\Omega}}$ . The column vectors  $\mathbf{B}_k$  with elements  $B_{jk}$  define the eigenvectors  $\Upsilon_k$  in terms of the basis functions  $\Psi_j$  as

$$\Upsilon_k = \sum_{j=1}^J B_{jk} \Psi_j, \quad (26)$$

assuming that the  $\Psi_j$ 's form a locally complete basis.

The matrix elements (24) can be expressed in terms of the signal  $c_n$ , the explicit knowledge of the auxiliary objects  $\hat{\Omega}$ ,  $\Upsilon_k$  or  $\Phi_0$  is not needed. Indeed, insertion of Eq. 23 into Eq. 24, use of the symmetry property,  $(\Psi, \hat{U}\Phi) = (\hat{U}\Psi, \Phi)$ , and the definition of  $c_n$ , Eq. 20, gives after some arithmetic

$$\begin{aligned} U^{(p)}(\varphi, \varphi') &= (e^{-i\varphi} - e^{-i\varphi'})^{-1} \left[ e^{-i\varphi} \sum_{n=0}^M e^{in\varphi'} c_{n+p} \right. \\ &\quad - e^{-i\varphi'} \sum_{n=0}^M e^{in\varphi} c_{n+p} - e^{iM\varphi} \sum_{n=M+1}^{2M} e^{i(n-M-1)\varphi'} c_{n+p} \\ &\quad \left. + e^{iM\varphi'} \sum_{n=M+1}^{2M} e^{i(n-M-1)\varphi} c_{n+p} \right], \quad \varphi \neq \varphi', \\ U^{(p)}(\varphi, \varphi) &= \sum_{n=0}^{2M} (M - |M - n| + 1) e^{in\varphi} c_{n+p}. \end{aligned} \quad (27)$$

(Note, that evaluation of  $\mathbf{U}^{(p)}$  requires knowledge of  $c_n$  for  $n = p, p+1, \dots, N = 2M+p$ .)

The solution of the generalized eigenvalue problem (25) is usually done by a singular value decomposition of the matrix  $\mathbf{U}^{(0)}$ . Each value of  $p$  yields a set of frequencies  $w_k$  and, due to Eqs. 22, 23 and 26, amplitudes,

$$d_k = \left( \sum_{j=1}^J B_{jk} \sum_{n=0}^M c_n e^{n\varphi_j} \right)^2. \quad (28)$$

Note that Eq. 28 is a functional of the half signal  $c_n, n = 1, 2, \dots, M$ . Even though in all our applications Eq. 28 gave very good results, we present here an even better expression for the coefficients  $d_k$  (see ref. [15]),

$$\begin{aligned} d_k &= \left[ \frac{1}{M+1} \sum_{j=1}^J B_{jk} (\Psi(\varphi_j), \Psi(w_k)) \right]^2 \\ &\equiv \left[ \frac{1}{M+1} \sum_{j=1}^J B_{jk} U^{(0)}(\varphi_j, w_k) \right]^2 \end{aligned} \quad (29)$$

with  $U^{(0)}(\varphi_j, w_k)$  defined by Eq. 27. Eq. 29 is a functional of the whole available signal  $c_n, n = 0, 1, \dots, 2M$ .

The converged  $w_k$  and  $d_k$  should not depend on  $p$ . This condition allows to identify spurious or non-converged frequencies by comparing the results with different values of



$p$  (e.g., with  $p = 1$  and  $p = 2$ ). We can define the simplest error estimate  $\varepsilon$  as the difference between the frequencies  $w_k$  obtained from diagonalizations with  $p = 1$  and  $p = 2$ , i.e.

$$\varepsilon = |w_k^{(p=1)} - w_k^{(p=2)}| . \quad (30)$$

## 4. Riemann zeros by harmonic inversion

### 4.1. Numerical results

For a numerical demonstration we construct the signal  $C_\sigma(s)$  using Eqs. 15 and 17 in the region  $s < \ln(10^6) = 13.82$  from the first 78498 prime numbers and with a Gaussian smoothing width  $\sigma = 0.0003$ . Parts of the signal are presented in Fig. 1. Up to  $s \approx 8$  the Gaussian approximations to the  $\delta$ -functions do essentially not overlap (see Fig. 1a) whereas for  $s \gg 8$  the mean spacing  $\Delta s$  between successive  $\delta$ -functions becomes much less than the Gaussian width  $\sigma = 0.0003$  and the signal fluctuates around the mean  $\overline{C}(s) = ie^{s/2}$  (see Fig. 1b). From this signal we were able to calculate about 2600 Riemann zeros to 12 digit precision. For the small generalized eigenvalue problem (25) we used matrices with dimension  $J < 100$ . To improve the numerical accuracy the matrices have been diagonalized with quadruple precision. Some Riemann zeros  $w_k$ , the corresponding amplitudes  $d_k$ , and the estimated errors  $\varepsilon$  (see Eq. (30)) are given in Tables 1 and 2. Within the numerical error the Riemann zeros are real and the amplitudes are consistent with  $d_k = 1$  for non-degenerate zeros. However, a few  $w_k$  have been revealed (see Table 3) which are definitely not located on the real axis. Except for the first at  $w = i/2$  they can be identified with the trivial real zeros of the zeta function at  $z = -2n$ ;  $n = 1, 2, \dots$ . The numerical accuracy for the trivial zeros decreases rapidly with increasing  $n$ . The value  $w = i/2$  in Table 3 is special because in this case the amplitude is negative, i.e.  $d_k = -1$ . Writing the zeta function in the form [17]

$$\zeta\left(\frac{1}{2} - iw\right) = C \prod_k (w - w_k)^{d_k} A(w, w_k) \quad (31)$$

where  $C$  is a constant and  $A$  a regularizing function which ensures convergence of the product, integer values  $d_k$  are the multiplicities of *zeros*. Therefore it is reasonable to relate negative integer values with the multiplicities of *poles*. In fact,  $\zeta(z)$  has a simple pole at  $z = \frac{1}{2} - iw = 1$  consistent with  $w = i/2$  in Table 3.

### 4.2. How many Riemann zeros can be obtained from a given set of primes?

We have calculated Riemann zeros by harmonic inversion of the signal  $C_\sigma(s)$  (Eq. 17) which uses prime numbers as input. The question arises how many Riemann zeros can

be converged for a given set of prime numbers. In general the required signal length  $s_{\max}$  for harmonic inversion is related to the average density of frequencies  $\bar{\varrho}(w)$  by [15]

$$s_{\max} \approx 4\pi\bar{\varrho}(w) . \quad (32)$$

With the average density of Riemann zeros derived from (4),

$$\bar{\varrho}(w) = \frac{d\bar{N}}{dw} = \frac{1}{2\pi} \ln\left(\frac{w}{2\pi}\right) \quad (33)$$

we obtain

$$s_{\max} = \ln(p_{\max}) = 2 \ln\left(\frac{w}{2\pi}\right) \Rightarrow p_{\max} = \left(\frac{w}{2\pi}\right)^2 . \quad (34)$$

The number of primes with  $p < p_{\max}$  can be estimated from the prime number theorem

$$\pi(p_{\max}) \sim \frac{p_{\max}}{\ln(p_{\max})} = \frac{(w/2\pi)^2}{2 \ln(w/2\pi)} . \quad (35)$$

On the other hand the number of Riemann zeros as a function of  $w$  is given by Eq. (4). The estimated number of Riemann zeros which can be obtained by harmonic inversion from a given set of primes is presented in Fig. 2. For example, about 80 zeros ( $w < 200$ ) can be extracted from the short signal  $C_{\sigma}(s)$  with  $s_{\max} = \ln(1000) = 6.91$  (168 prime numbers) in agreement with the estimates given above.

#### 4.3. A remark on the Riemann hypotheses

We conclude this Section with a remark on the famous Riemann hypotheses mentioned above. Applying our method of harmonic inversion to the signal  $C_{\sigma}(s)$  (Eq. 17) the Riemann hypotheses for the *zeros* of the zeta function,  $\zeta(z = \frac{1}{2} - iw_k) = 0$ , is directly related to an equivalent statement for the *eigenvalues*  $e^{-ipw_k}$  of the operator  $e^{-ip\tau\hat{\Omega}}$ , i.e., the generalized eigenvalue problem (25). Speculations that the operator  $\hat{\Omega}$  can be regarded as the Hamiltonian of a quantum mechanical system have been presented by Berry [5]. Unfortunately,  $\hat{\Omega}$  is not known as it is only defined implicitly by its matrix representation (27), which is a linear functional of the signal (17). However, the very fact that the Riemann zeros are obtained as eigenvalues of some matrix with analytically known coefficients is already intriguing.

### 5. Periodic orbit quantization

As mentioned in Section 2 the basic equation (8) used for the calculation of Riemann zeros has the same mathematical form as Gutzwiller's semiclassical trace formula. Both series, Eq. 8 and the periodic orbit sum (9), suffer from similar convergence problems in that they are absolutely convergent only in the complex half-plane outside the region

where the Riemann zeros or quantum eigenvalues, respectively, are located. As a consequence in a direct summation of periodic orbit contributions smoothing techniques must be applied resulting in low resolution spectra for the density of states [18]. To extract individual eigenstates the semiclassical trace formula has to be analytically continued to the region of the quantum poles. Here dynamical zeta functions have turned out to be of particular interest. One technique is to apply an approximate functional equation and generalize the Riemann-Siegel formula (13) to dynamical zeta functions [6, 7]. However, the semiclassical functional equation can only be applied to bound systems with real eigenvalues and the concept requires introduction of *pseudo-orbits*. Another technique for analytic continuation is to expand the dynamical zeta function, given as an infinite Euler product over entries from classical periodic orbits, in terms of the cycle length of the orbits [3, 19, 20, 21]. The *cycle-expansion* series is rapidly convergent if a complete symbolic dynamics exists and the contributions of long orbits are approximately shadowed by contributions of short orbits. A combination of the cycle-expansion method with a functional equation has been applied to bound systems in [22, 23].

In this Section we apply the same technique that we used for the calculation of Riemann zeros, to the calculation of semiclassical eigenenergies and resonances of physical systems by harmonic inversion of the Gutzwiller's periodic orbit sum for the propagator. The method only requires the knowledge of all orbits up to a sufficiently long but finite period and does not rely on either an approximate semiclassical functional equation or pseudo-orbits, nor does it depend on the existence of a symbolic code for the orbits. It may therefore be applied in general to a large variety of systems with an underlying chaotic, mixed, or even regular classical dynamics. The derivation of an expression for the recurrence function to be harmonically inverted is here analogous to that in Section 2.2.

Following Gutzwiller [1, 2] the semiclassical response function for chaotic systems is given by

$$g^{\text{sc}}(E) = g_0^{\text{sc}}(E) + \sum_{\text{po}} A_{\text{po}} e^{iS_{\text{po}}} , \quad (36)$$

where  $g_0^{\text{sc}}(E)$  is a smooth function and the  $S_{\text{po}}$  and  $A_{\text{po}}$  are the classical actions and weights (including phase information given by the Maslov index) of periodic orbit contributions. Eq. (36) is also valid for integrable [28] and near-integrable [29, 30] systems but with different expressions for the amplitudes  $A_{\text{po}}$ . The eigenenergies and resonances are the poles of the response function but unfortunately, its semiclassical approximation (36) does not converge in the region of the poles, thus the problem is the analytic continuation of  $g^{\text{sc}}(E)$  to this region.

In the following we assume that the classical system has a scaling property, i.e., the shape of periodic orbits does not depend on the scaling parameter,  $w$ , and the classical

action scales as

$$S_{\text{po}} = w s_{\text{po}} . \quad (37)$$

Examples of scaling systems are billiards [3, 24], Hamiltonians with homogeneous potentials [25, 26], Coulomb systems [20], or the hydrogen atom in external magnetic and electric fields [27, 21]. Quantization yields bound states or resonances,  $w_k$ , for the scaling parameter. In scaling systems the semiclassical response function  $g^{\text{sc}}(w)$  can be Fourier transformed easily to obtain the semiclassical trace of the propagator

$$C^{\text{sc}}(s) = \frac{1}{2\pi} \int_{-\infty}^{+\infty} g^{\text{sc}}(w) e^{-isw} dw = \sum_{\text{po}} A_{\text{po}} \delta(s - s_{\text{po}}) . \quad (38)$$

The signal  $C^{\text{sc}}(s)$  has  $\delta$ -peaks at the positions of the classical periods (scaled actions)  $s = s_{\text{po}}$  of periodic orbits and with peak heights (recurrence strengths)  $A_{\text{po}}$ , i.e.,  $C^{\text{sc}}(s)$  is Gutzwiller's periodic orbit recurrence function. Consider now the quantum mechanical counterparts of  $g^{\text{sc}}(w)$  and  $C^{\text{sc}}(w)$  taken as the sums over the poles  $w_k$  of the Green's function,

$$g^{\text{qm}}(w) = \sum_k \frac{d_k}{w - w_k + i\epsilon} , \quad (39)$$

$$C^{\text{qm}}(s) = \frac{1}{2\pi} \int_{-\infty}^{+\infty} g^{\text{qm}}(w) e^{-isw} dw = -i \sum_k d_k e^{-iw_k s} , \quad (40)$$

with  $d_k$  being the multiplicities of resonances, i.e.,  $d_k = 1$  for non-degenerate states. In analogy with the calculation of Riemann zeros from Eq. (17) the frequencies,  $w_k$ , and amplitudes,  $d_k$ , can now be extracted by harmonic inversion of the signal  $C^{\text{sc}}(s)$  after convoluting it with a Gaussian, i.e.

$$C_{\sigma}^{\text{sc}}(s) = \frac{1}{\sqrt{2\pi}\sigma} \sum_{\text{po}} A_{\text{po}} e^{(s-s_{\text{po}})^2/2\sigma^2} . \quad (41)$$

By fitting  $C_{\sigma}^{\text{sc}}(s)$  to the functional form of Eq. (40), the frequencies,  $w_k$ , can be interpreted as the semiclassical approximation to the poles of the Green's function in (39). Note that the harmonic inversion method described in Section 3 allows to study signals with complex frequencies  $w_k$ . For open systems the complex frequencies can be interpreted as semiclassical resonances. Note also that the  $w_k$  in general differ from the exact quantum eigenvalues because Gutzwiller's trace formula (36) is an approximation, correct only to first order in  $\hbar$ . Therefore the diagonalization of small matrices in (25) does not imply that the results of periodic orbit quantization are more "quantum" in any sense than those obtained, e.g., from a cycle expansion [3]. The eigenvalues are solutions of non-linear equations and the diagonalization is equivalent to the search of zeros of the dynamical zeta function in the cycle expansion technique. Numerical calculation of the zeros is also a non-linear problem and, in contrast to the matrix diagonalization, might encounter a problem of missing roots.

## 6. The three disk scattering system

Consider a billiard system which consists of three identical hard disks with unit radii,  $R = 1$ , displaced from each other by the same distance  $d$ . This simple, albeit nontrivial, scattering system has served as a model for periodic orbit quantization in many investigations during recent years [3, 31, 32, 33]. For  $d > 2.1$  the classical dynamics is completely hyperbolic, i.e., all periodic orbits are unstable and there are no bifurcations. After symmetry reduction the periodic orbits can be classified by a binary symbolic code [3]. For  $d = 6$  semiclassical resonances have been calculated by application of the cycle expansion technique including all periodic orbits up to cycle length  $n = 13$  [33]. In order to demonstrate the usefulness of our harmonic inversion technique we first apply it to the case  $R : d = 1 : 6$  studied before. Note that this corresponds to the very favorable regime for the cycle expansion (see below). In billiards the scaled action  $s$  is given by the length  $L$  of orbits ( $s = L$ ) and the quantized parameter is the absolute value of the wave vector  $k = |\mathbf{k}| = \sqrt{2mE}/\hbar$ . Fig. 3a shows the periodic orbit recurrence function, i.e., the trace of the semiclassical propagator  $C^{\text{sc}}(L)$ . The groups with oscillating sign belong to periodic orbits with adjacent cycle lengths. To obtain a smooth function on an equidistant grid, which is required for our harmonic inversion method, the  $\delta$ -functions in (38) have been convoluted with a Gaussian with width  $\sigma = 0.0015$ . As explained in Section 2 this does not change the underlying spectrum. The results of the harmonic inversion analysis of this signal are presented in Fig. 3b and Tables 4 and 5. The crosses in Fig. 3b represent semiclassical poles for which the amplitudes  $d_k$  are very close to 1 mostly within one percent. Because the amplitudes converge much slower than the frequencies these resonance positions are assumed to be very accurate within the semiclassical approximation. In fact, a perfect agreement to many significant figures is achieved for these poles with the results obtained by cycle expansion [33]. For some broad resonances marked by diamonds in Fig. 3b and Tables 4 and 5 the  $d_k$  deviate strongly from 1 within 5 to maximal 50 percent. It is not clear whether these strong deviations are due to numerical effects such as convergence problems caused by a too short signal, or if they are a direct consequence of the semiclassical approximation. Of course, with the exact expressions all multiplicities  $d_k$  should be 1 but there is no proof that this is still true within the semiclassical approximation. However, for the lowest  $k$  eigenvalues (see, e.g., the first three resonances in Table 4) where the agreement with the exact resonance energies is worst [33]  $d_k = 1$  still holds, indicating that there is no  $\hbar$ -dependence for the multiplicities.

The cycle expansion technique is based on the idea that the contributions of long periodic orbits are shadowed by those of short orbits. For the three disk scattering system this is ideally fulfilled in the limit of a large ratio  $d/R \gg 2$ . For short distances between the disks this is no longer true and hence the convergence of the conventional

cycle expansion is rather slow. For the ratio  $d/R = 3$  semiclassical resonances have been obtained from a sophisticated evaluation of the Selberg zeta function, where the leading pole of the zeta function was removed to improve the convergence of the cycle expansion [32]. The advantage of the periodic orbit quantization by harmonic inversion is that it does not depend on the existence of a symbolic code, the shadowing of orbits, and the removal of leading poles of Selberg’s zeta function.

As a second example of periodic orbit quantization by harmonic inversion we study the three disk scattering system with a challenging short distance ratio  $d/R = 2.5$  and thus in a situation where the assumption of the cycle expansion that contributions of long orbits are shadowed by short orbits is no longer a good approximation. The results are presented in Fig. 4 and Table 6. For large  $L$  groups of orbits with the same cycle length of the symbolic code strongly overlap and cannot be recognized in Fig. 4a. The signal is obtained from periodic orbits with cycle length  $n \leq 13$ . Note that only 356 periodic orbits with  $L < 7.5$  are included in the signal (Fig. 4a) whereas the complete set of orbits with cycle length  $n \leq 13$  consists of 1377 orbits.

## 7. Conclusion

We have introduced harmonic inversion as a new and general tool for semiclassical periodic orbit quantization and finding the roots of the Riemann and dynamical zeta functions. The method requires the complete set of periodic orbits up to a given maximum period as input but does not depend on special properties of the orbits, as, e.g., the existence of a symbolic code or a functional equation. Therefore the method can also serve as a tool for the semiclassical quantization of systems with mixed regular-chaotic classical dynamics which still is a challenging and unsolved problem. The signal  $C^{\text{sc}}(s)$  can be composed as the sum of a signal related to the irregular part of the classical phase space with periodic orbit amplitudes given by Gutzwiller’s trace formula [2] and a signal related to stable [28] or nearly integrable [29] torus structures. It should also be possible to include, e.g., creeping orbits [34], ghost orbit contributions [35, 36, 16], and higher order  $\hbar$  corrections [37] into the signal  $C^{\text{sc}}(s)$ , which can then be inverted to reveal the semiclassical poles. The method can even be used for a semiclassical periodic orbit quantization of systems with non-homogeneous potentials like the potential surfaces of molecules when a generalized scaling technique [38] is applied.

## Acknowledgments

We are grateful to B. Eckhardt who kindly communicated to us his periodic orbits for the three disk scattering system. J. M. thanks the Alexander von Humboldt-Stiftung for a Feodor-Lynen scholarship and H. Taylor and the University of Southern California

for their kind hospitality and support.

## References

- [1] Gutzwiller M C 1967 *J. Math. Phys.* **8** 1979 and 1971 *J. Math. Phys.* **12** 343
- [2] Gutzwiller M C 1990, *Chaos in Classical and Quantum Mechanics* (New York: Springer)
- [3] Cvitanović P and Eckhardt B 1989 *Phys. Rev. Lett.* **63** 823
- [4] Edwards H M 1974 *Riemann's Zeta function* (New York: Academic Press)
- [5] Berry M V 1986, Riemann's zeta function: A model for quantum chaos? *Quantum Chaos and Statistical Nuclear Physics*, ed T H Seligman and H Nishioka (*Lecture Notes in Physics* **263**) (Berlin: Springer) pp 1-17
- [6] Berry M V and Keating J P 1990 *J. Phys. A* **23** 4839
- [7] Keating J 1992 *Chaos* **2** 15
- [8] Bohigas O and Giannoni M J 1984 Chaotic motion and random-matrix theories *Mathematical and Computational Methods in Nuclear Physics* ed J S Dehesa J M G Gomez and A Polls (*Lecture Notes in Physics* **209**) (Berlin: Springer) pp 1-99
- [9] Odlyzko A M 1990 *The 10<sup>20</sup>th zero of the Riemann zeta function and 70 million of its neighbours* (AT&T Bell Laboratories)
- [10] Bogomolny E and Keating J 1995 *Nonlinearity* **8** 1115
- [11] Main J, Mandelshtam V A, and Taylor H S 1997 *Phys. Rev. Lett.* **79** 825
- [12] Marple S, Jr. 1987, *Digital Spectral Analysis with Applications*, Prentice-Hall, Englewood Cliffs
- [13] Wall M R and Neuhauser D 1995 *J. Chem. Phys.* **102** 8011
- [14] Mandelshtam V A and Taylor H S 1997 *Phys. Rev. Lett.* **78** 3274
- [15] Mandelshtam V A and Taylor H S 1997 *J. Chem. Phys.* submitted
- [16] Main J, Mandelshtam V A, and Taylor H S 1997 *Phys. Rev. Lett.* **78** 4351
- [17] Titchmarsh E C 1986 *The Theory of the Riemann Zeta-Function* OUP, 2nd ed.
- [18] Wintgen D 1988 *Phys. Rev. Lett.* **61** 1803
- [19] Ezra G S, Richter K, Tanner G, and Wintgen D 1991 *J. Phys. B* **24** L413
- [20] Wintgen D, Richter K, and Tanner G 1992 *Chaos* **2** 19
- [21] Tanner G, Hansen K T, and Main J 1996 *Nonlinearity* **9** 1641
- [22] Tanner G, Scherer P, Bogomolny E B, Eckhardt B, and Wintgen D 1991 *Phys. Rev. Lett.* **67** 2410
- [23] Tanner G and Wintgen D 1992 *Chaos* **2** 53
- [24] Heller E J 1984 *Phys. Rev. Lett.* **53** 1515
- [25] Martens C C, Waterland R L, and Reinhardt W P 1989 *J. Chem. Phys.* **90** 2328
- [26] Tomsovic S 1991 *J. Phys. A* **24** L733
- [27] Main J, Wiebusch G, Welge K H, Shaw J, and Delos J B (1994) *Phys. Rev. A* **49** 847
- [28] Berry M V and Tabor M 1976 *Proc. R. Soc. London* **A349** 101
- [29] Tomsovic S, Grinberg M, and Ullmo D 1995 *Phys. Rev. Lett.* **75** 4346
- [30] Ullmo D, Grinberg M, and Tomsovic S 1996 *Phys. Rev. E* **54** 136
- [31] Gaspard P and Rice S A 1989 *J. Chem. Phys.* **90** 2225, 2242, and 2255
- [32] Eckhardt B and Russberg G 1993 *Phys. Rev. E* **47** 1578
- [33] Eckhardt B, Cvitanović P, Rosenqvist P, Russberg G, and Scherer P 1995 Pinball Scattering, in *Quantum Chaos*, ed G Casati and B V Chirikov, (Cambridge: University Press), pp 405-434
- [34] Wirzba A 1992 *Chaos* **2** 77

- [35] Kuś M, Haake F, and Delande D 1993 *Phys. Rev. Lett.* **71** 2167
- [36] Main J and Wunner G 1997 *Phys. Rev. A* **55** 1743
- [37] Gaspard P and Alonso D 1993 *Phys. Rev. A* **47** R3468
- [38] Main J, Jung C, and Taylor H S 1997 *J. Chem. Phys.* in press



## Figures and Tables

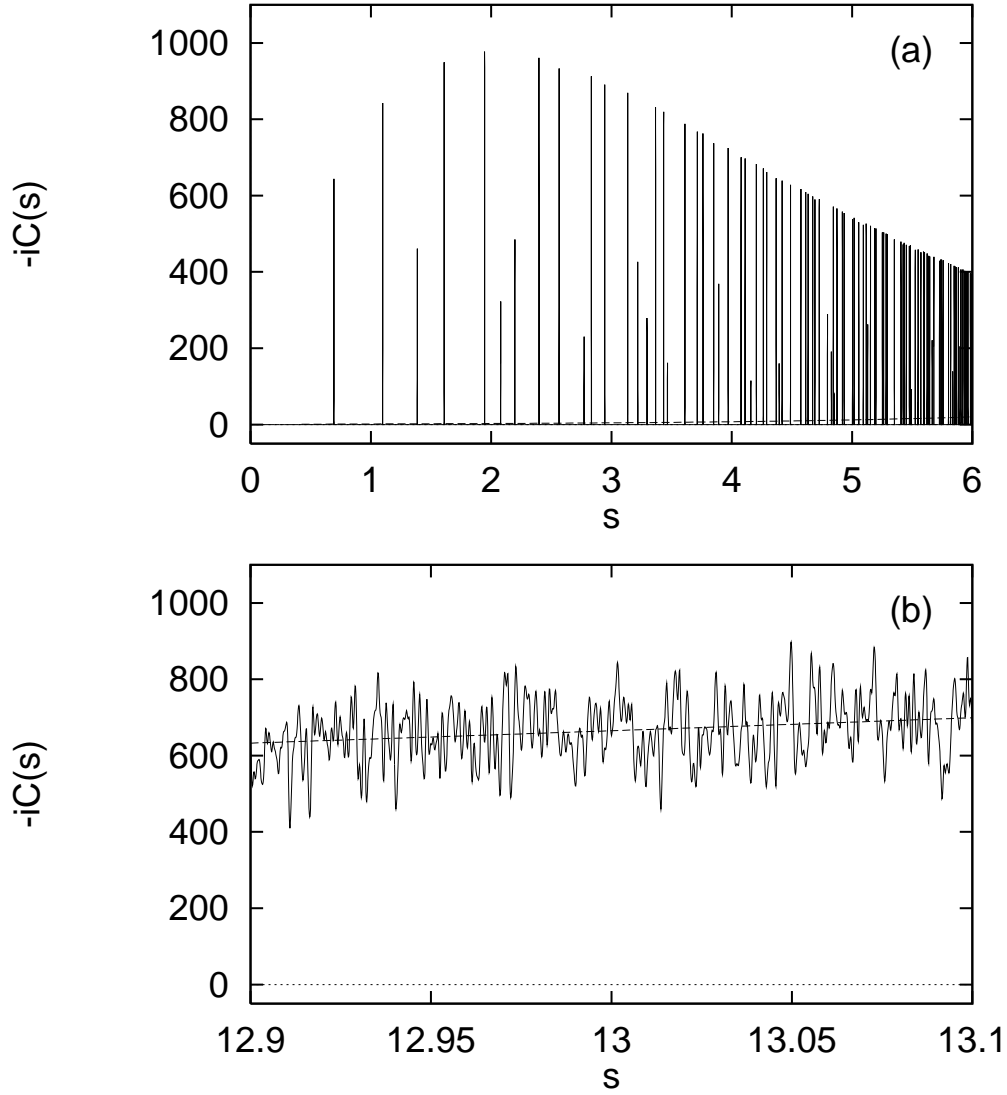


**Figure 1.** “Recurrence” function  $-iC_\sigma(s)$  for the Riemann zeros which has been analyzed by harmonic inversion. (a) Range  $0 \leq s \leq 6$ , (b) short range around  $s = 13$ . The  $\delta$ -functions have been convoluted by a Gaussian with width  $\sigma = 0.0003$ . Dashed line: Smooth background  $\overline{C}(s) = ie^{s/2}$  resulting from the pole of the zeta function.

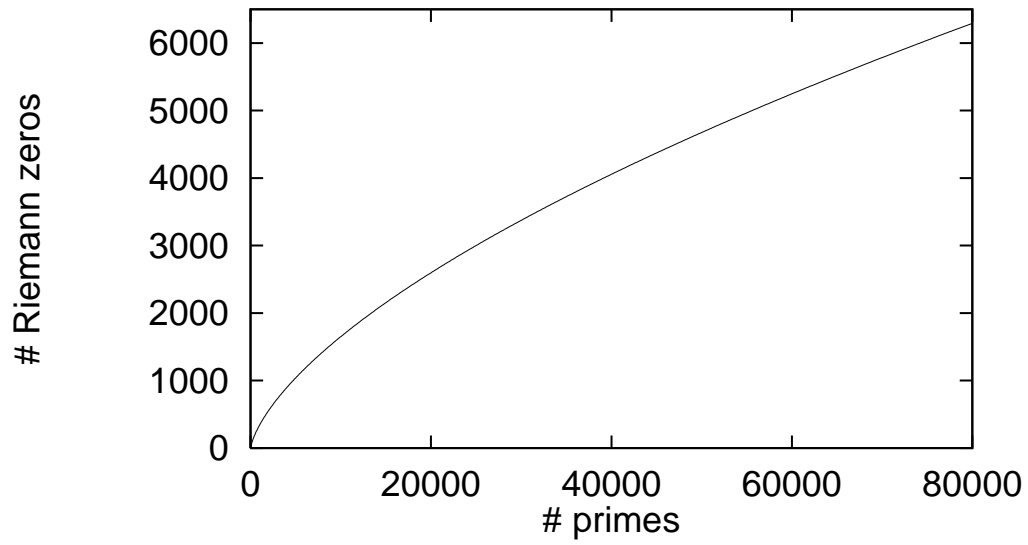


**Figure 2.** Estimated number of converged zeros of the Riemann zeta function which can be obtained for given number of primes  $p$ .

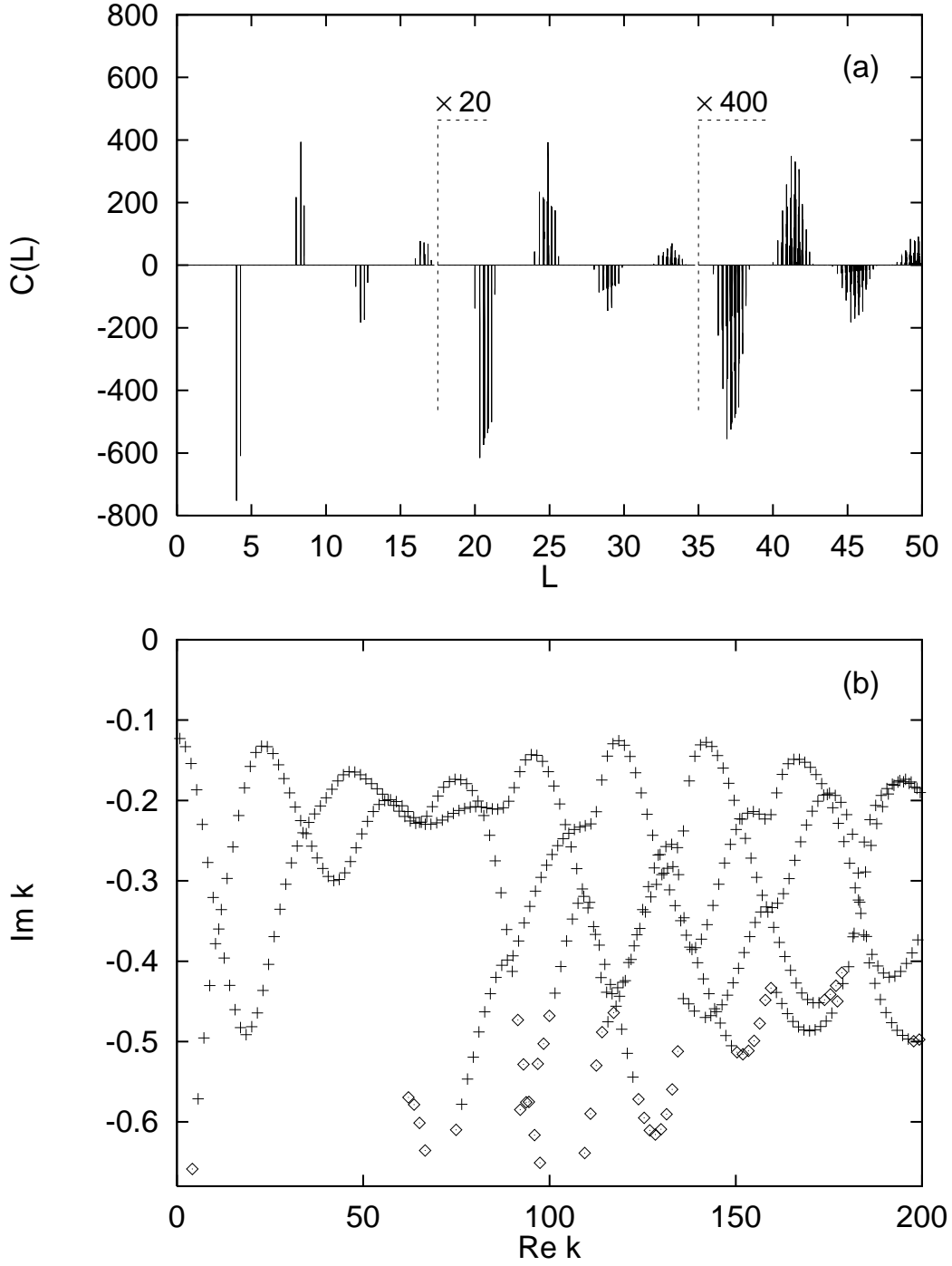


**Figure 3.** Three disk scattering system ( $A_1$  subspace) with  $R = 1$ ,  $d = 6$ . (a) Periodic orbit recurrence function,  $C(L)$ . The signal has been convoluted with a Gaussian of width  $\sigma = 0.0015$ . (b) Semiclassical resonances. The resonance positions marked by diamonds might be less accurate (see text).

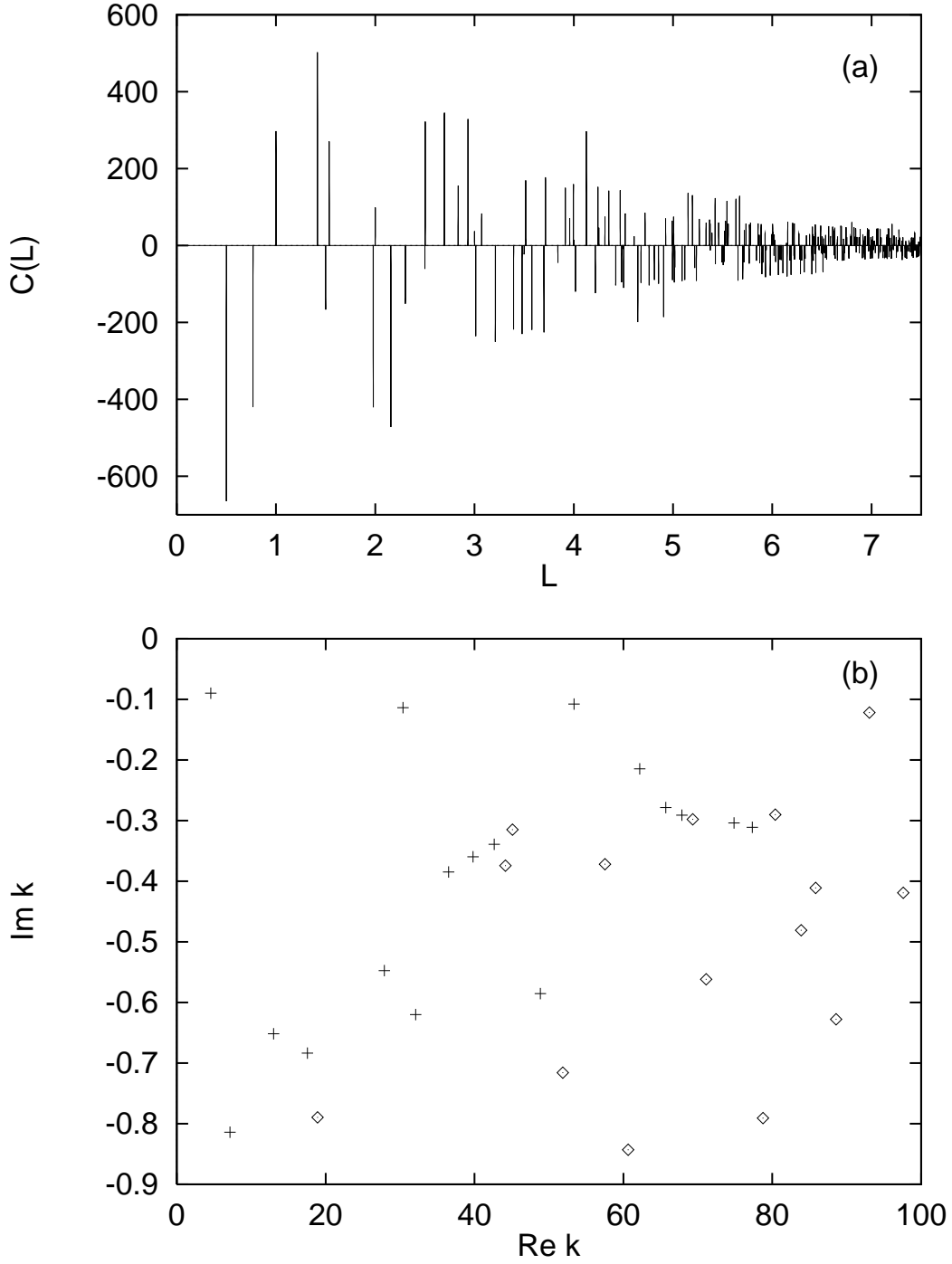


**Figure 4.** Three disk scattering system ( $A_1$  subspace) with  $R = 1$ ,  $d = 2.5$ . (a) Periodic orbit recurrence function,  $C(L)$ . The signal has been convoluted with a Gaussian of width  $\sigma = 0.0003$ . (b) Semiclassical resonances. The resonance positions marked by diamonds might be less accurate (see text).

**Table 1.** Non-trivial zeros  $w_k$ , multiplicities  $d_k$ , and error estimate  $\varepsilon$  for the Riemann zeta function.

$k$	Re $w_k$	Im $w_k$	Re $d_k$	Im $d_k$	$\varepsilon$
1	14.13472514	4.05E-12	1.00000011	-5.07E-08	3.90E-13
2	21.02203964	-2.23E-12	1.00000014	1.62E-07	9.80E-13
3	25.01085758	1.66E-11	0.99999975	-2.64E-07	5.20E-12
4	30.42487613	-6.88E-11	0.99999981	-1.65E-07	1.90E-12
5	32.93506159	7.62E-11	1.00000020	5.94E-08	7.10E-13
6	37.58617816	1.46E-10	1.00000034	5.13E-07	1.00E-12
7	40.91871901	-3.14E-10	0.99999856	1.60E-06	4.90E-11
8	43.32707328	1.67E-11	1.00000008	3.29E-07	1.90E-12
9	48.00515088	4.35E-11	0.99999975	-1.35E-07	1.40E-12
10	49.77383248	7.02E-11	1.00000254	-4.59E-07	1.10E-10
11	52.97032148	1.92E-10	1.00000122	7.31E-07	6.00E-11
12	56.44624770	-1.30E-10	0.99999993	4.51E-07	5.50E-12
13	59.34704400	5.40E-11	0.99999954	2.34E-06	2.30E-10
14	60.83177852	-3.94E-10	1.00000014	1.11E-06	3.00E-11
15	65.11254406	-4.98E-09	0.99998010	-8.30E-06	2.70E-08
16	67.07981053	-2.05E-10	0.99999892	-8.04E-07	5.30E-11
17	69.54640171	2.51E-11	0.99999951	9.45E-07	6.80E-12
18	72.06715767	-5.74E-10	0.99999974	8.63E-06	4.30E-10
19	75.70469070	3.93E-10	1.00000082	1.07E-06	3.20E-11
20	77.14484007	-2.70E-12	0.99999979	1.25E-06	1.30E-11
21	79.33737502	-3.58E-11	1.00000086	3.03E-07	9.20E-12
22	82.91038085	1.56E-10	0.99999912	-8.58E-07	1.60E-11
23	84.73549298	3.34E-10	0.99999940	-7.09E-07	2.50E-11
24	87.42527461	1.20E-09	0.99999866	1.39E-06	6.70E-11
25	88.80911121	-9.42E-10	1.00000101	1.49E-06	4.80E-11
26	92.49189927	-4.11E-09	0.99999761	-1.93E-06	1.50E-10
27	94.65134404	-7.11E-09	1.00000520	-1.27E-06	6.80E-10
28	95.87063426	8.06E-09	0.99999001	-1.15E-05	5.20E-09
29	98.83119422	-1.78E-11	0.99999936	5.70E-07	3.10E-12
30	101.31785101	4.22E-11	0.99999969	-4.73E-07	4.50E-12

**Table 2.** Non-trivial zeros  $w_k$ , multiplicities  $d_k$ , and error estimate  $\varepsilon$  for the Riemann zeta function.

$k$	Re $w_k$	Im $w_k$	Re $d_k$	Im $d_k$	$\varepsilon$
2531	3063.43508648	-1.64E-09	0.99999901	1.34E-06	5.50E-11
2532	3065.28655558	1.15E-09	1.00000107	-3.63E-07	2.40E-11
2533	3066.32025039	-1.66E-10	1.00000231	1.00E-06	1.20E-10
2534	3067.07132023	3.68E-09	1.00000334	2.73E-07	2.20E-10
2535	3068.01350133	-1.51E-09	1.00000291	1.46E-06	2.10E-10
2536	3068.98426618	-5.92E-09	1.00000205	2.94E-06	2.60E-10
2537	3069.78290477	-4.40E-09	1.00000237	2.51E-06	2.40E-10
2538	3070.54262154	-7.71E-10	1.00000169	9.57E-07	7.90E-11
2539	3072.00099337	-6.44E-11	0.99999908	2.17E-07	2.00E-11
2540	3073.18523777	9.17E-11	0.99999942	-1.07E-06	3.00E-11
2541	3074.52349428	6.73E-09	1.00000391	-6.51E-07	3.50E-10
2542	3075.03387288	-1.22E-08	1.00000117	-5.69E-06	7.30E-10
2543	3075.83347924	-3.13E-09	1.00000013	-3.86E-06	3.10E-10
2544	3077.42747330	5.76E-10	1.00000561	4.69E-06	1.10E-09
2545	3078.28622690	1.34E-08	1.00001283	1.10E-06	3.80E-09
2546	3078.89737915	1.61E-09	1.00000487	-8.04E-06	2.10E-09
2547	3079.87139464	1.70E-09	1.00000275	-2.32E-06	3.00E-10
2548	3080.85638233	8.67E-10	1.00000159	-4.12E-07	5.90E-11
2549	3082.16316375	-5.88E-10	1.00000013	8.44E-07	1.70E-11
2550	3083.36135798	8.43E-10	0.99999923	3.45E-07	1.50E-11
2551	3084.83845150	2.72E-09	1.00000057	-2.86E-06	1.80E-10
2552	3085.37726898	-1.37E-08	0.99999576	-2.88E-06	5.50E-10
2553	3085.96552225	6.39E-09	0.99999667	1.50E-06	2.80E-10
2554	3087.01881535	3.46E-11	0.99999845	-3.63E-07	5.20E-11
2555	3088.08343703	-3.89E-10	0.99999931	-8.44E-07	2.40E-11
2556	3089.22230894	-3.31E-10	1.00000017	-9.21E-07	1.80E-11
2557	3090.28219490	2.97E-10	1.00000069	-7.17E-07	2.10E-11
2558	3091.15446969	1.10E-09	1.00000052	-6.59E-07	1.50E-11
2559	3092.68766704	2.25E-09	1.00000033	1.45E-06	5.20E-11
2560	3093.18544571	-2.33E-09	1.00000168	-1.50E-07	6.40E-11

**Table 3.** Trivial zeros and pole of the Riemann zeta function.

Re $w_k$	Im $w_k$	Re $d_k$	Im $d_k$	$\varepsilon$
0.00000000	0.50000000	-1.00000002	-4.26E-08	1.80E-14
-0.00000060	-2.49999941	0.99992487	-3.66E-05	1.80E-07
-0.00129915	-4.49987911	1.00069939	-3.25E-03	4.40E-05
-0.09761173	-6.53286064	1.07141445	-1.49E-01	1.70E-03

**Table 4.** Semiclassical resonances, multiplicities, and error estimates for the three disk scattering problem ( $A_1$  subspace) with  $R = 1$ ,  $d = 6$ . The marked resonances are plotted as diamonds in Fig. 3b.

Re $k$	Im $k$	Re $d$	Im $d$	$\varepsilon$
0.75831390	-0.12282220	0.99999998	-0.00000001	2.84E-12
2.27427857	-0.13305873	1.00000000	0.00000000	2.71E-14
3.78787678	-0.15412739	1.00000001	0.00000000	1.11E-13
◇ 4.14568980	-0.65853972	0.94261284	-0.05782200	1.79E-06
5.29606778	-0.18678731	1.00000000	0.00000004	2.63E-12
5.68149760	-0.57137210	0.99512763	-0.01739098	5.34E-07
6.79363653	-0.22992212	0.99999994	0.00000018	1.54E-11
7.22405797	-0.49542427	1.00092001	-0.00461967	4.02E-07
8.27639062	-0.27708051	1.00000064	-0.00000007	3.47E-11
8.77921337	-0.43025611	0.99900081	0.00120544	1.00E-07
9.74763287	-0.32081704	0.99999986	0.00000049	6.32E-12
10.34422566	-0.37819884	1.00000189	0.00001109	3.89E-10
11.21347781	-0.35996394	1.00000180	-0.00000402	3.87E-10
11.91344955	-0.33573455	0.99999831	-0.00000066	2.50E-10
12.67753189	-0.39611536	0.99997860	-0.00000736	3.04E-09
13.48264892	-0.29694775	1.00000038	-0.00000054	6.90E-11
14.14241358	-0.43006040	1.00007802	0.00008149	2.54E-08
15.04730502	-0.25783568	0.99999988	-0.00000019	2.22E-11
15.61144308	-0.46038384	0.99664400	0.00551842	4.20E-06
16.60255984	-0.21887313	0.99999994	-0.00000023	2.05E-11
17.08755573	-0.48267959	0.99627755	-0.00253061	7.36E-07
18.14650089	-0.18423186	0.99999997	-0.00000024	2.51E-11
18.57339044	-0.49136421	0.99814244	0.00673976	6.94E-07
19.68083747	-0.15759269	1.00000003	-0.00000170	8.23E-10
20.06797545	-0.48149593	0.95226981	-0.02890527	2.10E-06
21.20806335	-0.14030860	1.00000000	-0.00000007	5.94E-13
21.57364133	-0.46433513	1.00085826	-0.00009476	1.01E-08
22.72965806	-0.13234332	1.00000002	0.00000000	6.48E-14
23.08723570	-0.43634339	1.00012288	-0.00014566	2.98E-09
24.24587785	-0.13311356	0.99999996	0.00000004	1.41E-12
24.60798811	-0.40389765	1.00005878	-0.00021677	6.02E-09
25.75604970	-0.14152648	0.99999994	-0.00000001	8.26E-13
26.13536838	-0.36944525	1.00011315	-0.00008199	4.27E-09
27.25924331	-0.15562722	0.99999986	-0.00000001	2.52E-12
27.66943857	-0.33534291	1.00005367	0.00000812	1.45E-09
28.75535257	-0.17275055	0.99999980	-0.00000013	4.83E-12
29.20982351	-0.30415273	0.99997593	0.00001914	1.06E-09



**Table 5.** Semiclassical resonances, multiplicities, and error estimates for the three disk scattering problem ( $A_1$  subspace) with  $R = 1$ ,  $d = 6$ . The marked resonances are plotted as diamonds in Fig. 3b.

	Re $k$	Im $k$	Re $d$	Im $d$	$\varepsilon$
	120.09660752	-0.13132401	1.00014269	-0.00002012	5.01E-09
	120.36157953	-0.42422813	0.99802782	-0.02405030	4.84E-07
	120.89414390	-0.51457342	1.00111789	-0.04368683	5.37E-07
	121.26449704	-0.40174847	0.99857960	0.00455485	8.11E-08
	121.61587346	-0.14515721	1.00000001	0.00000172	3.86E-11
	121.91578388	-0.39794687	1.00342693	-0.00124926	5.36E-08
◇	122.39332209	-0.54416152	1.02054670	-0.06474747	5.41E-07
	122.75339677	-0.38095471	0.99922123	0.00234143	2.84E-08
	123.13459298	-0.16565462	0.99999703	0.00000231	7.56E-11
	123.46800892	-0.36727762	1.00046828	0.00174180	2.51E-08
◇	123.89166973	-0.57174339	1.06644392	-0.10849630	1.17E-06
	124.24239698	-0.35938298	1.00003913	0.00147211	2.04E-08
	124.65207385	-0.19059475	0.99999152	0.00000344	1.84E-10
	125.01914206	-0.33583448	0.99925704	0.00038552	1.20E-08
◇	125.39246168	-0.59503215	1.14947103	-0.15202423	2.14E-06
	125.73060952	-0.33868744	1.00035374	0.00089953	1.76E-08
	126.16812780	-0.21726568	0.99997532	0.00000523	6.34E-10
	126.57000032	-0.30717994	0.99969830	-0.00028769	6.87E-09
◇	126.89863330	-0.61058335	1.24854908	-0.16290432	3.18E-06
	127.21759681	-0.32010287	1.00042752	0.00045232	1.30E-08
	127.68308651	-0.24341398	0.99993610	-0.00000236	2.13E-09
	128.12116088	-0.28389637	1.00010175	-0.00022229	4.95E-09
◇	128.41137217	-0.61577414	1.32422538	-0.11565068	4.11E-06
	128.70334065	-0.30442655	1.00039570	0.00011310	8.78E-09
	129.19732946	-0.26788859	0.99987656	-0.00004493	5.25E-09
	129.67319699	-0.26717842	1.00017817	0.00002664	4.62E-09
◇	129.92927207	-0.60918315	1.33322988	-0.02170382	4.76E-06
	130.18796223	-0.29223540	1.00028313	-0.00012743	6.65E-09
	130.71098079	-0.29045241	0.99983213	-0.00012609	8.19E-09
	131.22717821	-0.25736473	1.00000071	0.00017324	5.54E-09
◇	131.44889208	-0.59054385	1.26610320	0.06973001	4.99E-06
	131.67139581	-0.28429711	1.00010065	-0.00027624	6.60E-09

**Table 6.** Semiclassical resonances, multiplicities, and error estimates for the three disk scattering problem ( $A_1$  subspace) with  $R = 1$ ,  $d = 2.5$  obtained from the signal  $C(L)$  with  $L < 7.5$  in Fig. 4a. The marked resonances are plotted as diamonds in Fig. 4b.

Re $k$	Im $k$	Re $d$	Im $d$	$\varepsilon$
4.58122247	-0.08999148	1.00000417	0.00120203	6.97E-08
7.14266960	-0.81391029	1.01834965	-0.00823113	3.51E-06
12.99951105	-0.65166427	1.00042048	-0.00056855	1.31E-06
17.56322689	-0.68356906	0.98459703	-0.03060711	2.28E-05
◇ 18.91024231	-0.78956816	1.03497867	-0.07209360	6.09E-05
27.88792868	-0.54737225	1.02353431	0.00393194	2.30E-05
30.38871017	-0.11367391	1.00121948	0.00747117	2.68E-06
32.09837318	-0.62004177	0.99002266	0.01368255	3.50E-05
36.50721098	-0.38489303	1.00136214	0.01015558	9.58E-06
39.81154707	-0.35977801	1.00778064	-0.00596526	7.00E-05
42.65696984	-0.33910875	0.95316803	0.02942369	1.81E-05
◇ 44.15561123	-0.37442367	0.70366781	-0.27927232	9.13E-05
◇ 45.09670413	-0.31506305	0.77286261	0.10564855	2.54E-05
48.84367280	-0.58547564	0.97205165	0.01832879	3.83E-06
◇ 51.85539738	-0.71582111	1.05998879	-0.22754826	7.06E-05
53.36884896	-0.10779998	1.03903158	-0.03195638	7.48E-06
◇ 57.52623296	-0.37200326	0.54480246	0.04947934	6.95E-05
◇ 60.63258604	-0.84290683	1.12993346	0.06170742	4.50E-05
62.20192292	-0.21464518	1.00384284	0.02041431	3.04E-06
65.68454001	-0.27861785	1.02584325	0.03420385	5.51E-06
67.86305728	-0.29098741	1.01748508	-0.01128120	6.19E-06
◇ 69.32700248	-0.29789188	0.91331209	-0.06283737	5.73E-06
◇ 71.11378807	-0.56166741	1.04431265	0.20817721	4.26E-06
74.85580547	-0.30392250	1.00774480	0.01774683	8.79E-07
77.31348462	-0.31110834	0.98293492	-0.00865456	5.06E-06
◇ 78.74676605	-0.79088169	0.57558136	-0.30381968	1.39E-04
◇ 80.39325912	-0.29001165	0.67726720	-0.02534165	3.99E-05
◇ 83.89182348	-0.48077936	0.83497221	0.04875474	7.22E-05
◇ 85.81836634	-0.41116853	0.97551535	0.10003934	1.05E-05
◇ 88.57708414	-0.62777143	0.72880937	0.41114777	2.73E-05
◇ 93.03487282	-0.12178427	0.98433404	0.07997697	9.37E-05
◇ 97.58490354	-0.41923521	0.98663823	0.14408254	7.12E-05